IEEE Access
Multidisciplinary | Rapid Review | Open Access Journal

Date of publication xxxx 00, 0000, date of current version xxxx 00, 0000.

Digital Object Identifier 10.1109/ACCESS.2017.DOI

$SE(3)$ based LTV-MPC algorithm for multi-obstacle trajectory tracking of fully driven spacecraft

WENBANG WANG[1], XIAOKANG PENG[2], JIA AI[3], CHENG FU[1], CHAOBO LI[1] and ZEJIAN ZHANG[4]

[1]Hubei University of Technology, Wuhan 430068, China
[2]Shanghai Mechanical and Electrical Engineering Institute, Shanghai 200000, China
[3]Wuhan Railway Vocational College of Technology, Wuhan 430074, China
[4]Hubei Institute of Logistic Technology, Xiangyang, Hubei, China

Corresponding author: JIA AI (e-mail: aijia@wru.edu.cn.)

ABSTRACT

A linear time-varying model predictive control (LTV-MPC) method based on $SE(3)$ is proposed, to solve the problem of the control accuracy and energy consumption of spacecraft. First, left-invariant principle of Lie group, Lie algebra $SO(3)$, and other differential geometry theories are applied to extend LTV-MPC to $SE(3)$. Then, considering the obstacle avoidance problem of the spacecraft in space, a suitable optimization function is selected to ensure smooth tracking of the desired working trajectory. By controlling the incremental output with the fastest convergence rate, the controller enables effective trajectory tracking. Finally, the effectiveness and applicability of the controller are verified by simulation experiments. These simulations validate the controller's ability to achieve constraint satisfaction, optimize transient processes, and enhance control accuracy. The results provide compelling evidence of the controller's potential for real-world spacecraft control applications.

INDEX TERMS LTV-MPC; $SE(3)$; Spacecraft; Obstacle avoidance; Trajectory tracking.

I. INTRODUCTION

WITH the development of aerospace technology, spacecraft is widely used in space junk management and formation flights [1]–[3]. However, as space missions become more complex, the requirements for attitude and orbit control accuracy of spacecraft have gradually increased [4]–[6]. Conventional methods typically employ separate modeling and control techniques to address the attitude and orbital motions of a spacecraft, thereby simplifying the complexity of the problem [7], [8]. This method does not consider the coupling between the spacecraft's attitude and position, resulting in the control accuracy and response speed of the spacecraft struggling to meet mission requirements. In addition, considering that the spacecraft needs to avoid space obstacles during the mission, a further increase in the control accuracy of the spacecraft is required. Hence, it is necessary to develop a control method with higher accuracy for attitude and orbit integration.

In recent years, the spacecraft's attitude and orbit integration modeling method is mainly based on Euler angles, Rodrigues parameters, modified Rodrigues parameters and pairwise quaternions [9]–[11]. Compared with Euler angles and Rodrigues parameters, $SE(3)$ provides global, concise, and compact attitude expression without singularities. Compared with pairwise quaternions, $SE(3)$ is not characterized by ambiguity and receding winding, which can reduce the response speed of spacecraft control and increase energy consumption in practical applications. In addition, $SE(3)$ provides a solution to the challenges of ambiguity and recession that arise when describing the attitude of a rigid body within the integrated modeling of both attitude and orbit. There is a lot of research on $SE(3)$ in the spacecraft field [12]–[14]. In reference [12], an autonomous rendezvous and docking scheme for spacecraft is presented, which utilizes a robust adaptive terminal sliding mode approach grounded on $SE(3)$ modeling. In [13], a control law for spacecraft coupled tracking maneuvers is introduced, specifically addressing scenarios involving significant uncertainties in inertial parameters and external perturbations. This control law employs an adaptive timing terminal sliding mode method

based on the arrival law. However, the above methods still suffer from low control accuracy and poor robustness. In practical applications, these methods increase the energy consumption to satisfy the mission requirements.

Model Predictive Control (MPC) is a control strategy that utilizes the mathematical model of a system to predict its future behavior and make control decisions based on these predictions [14]. Recognized for its stability and robustness, MPC finds extensive applications in the field of control [15]–[17]. In [15], MPC is employed to establish motion control laws for addressing control challenges in complex, highly articulated robotic systems. In [16], MPC is applied to ensure the safe operation of spacecraft under extreme conditions, contributing to the development of spacecraft control architectures. Additionally, in [17], MPC is designed to tackle fuel consumption and performance tuning issues in spacecraft, showcasing its versatility in addressing diverse control problems. However, in practical applications, spacecraft often need to consider the time-varying nature of the system. To address this issue, a Linear Time-Varying Model Predictive Control (LTV MPC) is proposed, which proves more suitable for situations where the system undergoes dynamic changes compared to traditional MPC [18]. In [19], an LTV-MPC method is designed to solve the attitude control problem of satellites, achieving high-precision attitude control. Nevertheless, a common issue in the mentioned literature is the reliance on traditional quaternion modeling. The more advantageous $SE(3)$ modeling method, due to restrictions imposed by specific geometric shapes, faces challenges in integration with MPC. In this context, Kolmanovsky et al. apply MPC to the integration of spacecraft attitude and orbit, utilizing the $SE(3)$ framework to describe the system dynamics [20]. However, the linear model in this approach can only be effectively formulated near the origin, making it challenging to address global issues. Moreover, the method requires solving algebraic Riccati equations, introducing significant computational complexity limitations.

Furthermore, during spacecraft operations, obstacles such as other spacecraft or space debris may appear along the orbit. In such situations, to ensure a safer mission completion through effective obstacle avoidance, it is imperative to simultaneously consider state constraints and terminal constraints, addressing optimal control problems on $SE(3)$ [21]–[23]. In [21], the obstacle avoidance problem for autonomous spacecraft rendezvous and docking is solved based on the Gaussian function approach to designing the obstacle avoidance function. In [22], a non-linear optimization method based on model control is proposed to solve the spacecraft obstacle avoidance problem in the face of multiple and moving obstacles. However, the above methods still suffer from serious non-linearity and low computational efficiency.

In summary, this paper applies LTV-MPC to $SE(3)$ based on the left-invariant principle of the Lie group, the Lie algebra $so(3)$ and other differential geometry theories. In practical applications, it can effectively improve the control accuracy, and response speed and optimize fuel consumption. In addition, information about the obstacles in the spacecraft trajectory is considered and a suitable optimization function is selected to smoothly track the desired trajectory at the fastest convergence rate by controlling the incremental output. The main contributions in this paper are shown as follows:

1) Compared with reference [9]–[11], the design of a linear time-varying model predictive control based on $SE(3)$ addresses the limitations of existing controllers, such as low control accuracy and limited robustness.
2) Compared with reference [15]–[17], for reducing the energy consumption, the linear time-varying predictive control scheme is proposed, leading to improved overall efficiency.
3) Compared with reference [21]–[23], this paper considers the obstacle avoidance problem in spacecraft control and selects an appropriate optimization function to effectively handle the nonlinear characteristic of the problem while enhancing computational efficiency.

The subsequent sections of this paper are organized as follows: In Section 2, the attitude orbit integration model based on $SE(3)$ and the LTV-MPC design method in Euclidean space are presented. In Section 3, the program design of LTV-MPC on $SE(3)$ is explained, taking into account space obstacles. Additionally, the feasibility and stability proof of the algorithm is provided. In Section 4, simulation experiments are carried out to demonstrate the effectiveness of the proposed controller. In Section 5, a summary of the results obtained in this paper is provided.

II. PROBLEM STATEMENTS

A. DERIVATION OF THE DYNAMIC MODEL FOR SPACECRAFT

In this section, a detailed description of the derivation process of the spacecraft model is proposed. To describe the configuration of a spacecraft accurately, we utilize the special Euclidean group $SE(3)$, which is a Lie group containing the attitude and position of the spacecraft.

$$SO(3) = \{R \in \mathbb{R}^{3\times3} | R^T R = I, \det[R] = 1\} \tag{1}$$

where $R \in SO(3)$ represents the attitude of the spacecraft in the inertial reference frame. The spacecraft's configurations with respect to the inertial frame are described as follow:

$$g = \begin{bmatrix} R & p \\ 0_{1\times3} & 1 \end{bmatrix} \tag{2}$$

where $g \in SE(3)$ is used to describe the configuration of a spacecraft. The kinematic of the spacecraft based on $SE(3)$ is expressed as:

$$\dot{g} = g\bar{\varpi} \tag{3}$$

where $\varpi \in \mathbb{R}^6$ is the generalized velocity and can be described as:

$$\varpi = \begin{bmatrix} \Omega \\ V \end{bmatrix} \in \mathbb{R}^6 \tag{4}$$

where $\Omega \in \mathbb{R}^3$, $V \in \mathbb{R}^3$ are the angular and translational velocities in the body-fixed frame, respectively. $\bar{\varpi}$ is the generalized velocity and can be described as:

$$\bar{\varpi} = \begin{bmatrix} \Omega \\ V \end{bmatrix}^{-} = \begin{bmatrix} \hat{\Omega} & V \\ 0_{1\times 3} & 0 \end{bmatrix} \tag{5}$$

where $[\cdot]^{\wedge} : \mathbb{R}^3 \to so(3)$ is the antisymmetric matrix operation, $\hat{\Omega} \in SO(3)$ can be described as:

$$\hat{\Omega} = \begin{bmatrix} \Omega_1 \\ \Omega_2 \\ \Omega_3 \end{bmatrix}^{\wedge} = \begin{bmatrix} 0 & -\Omega_3 & \Omega_2 \\ \Omega_3 & 0 & \Omega_1 \\ -\Omega_2 & \Omega_1 & 0 \end{bmatrix} \tag{6}$$

The inverse of the hat map is defined as $[\cdot]^{\vee} : so(3) \to \mathbb{R}^3$, which is the vee map.

The dynamics equation of the spacecraft based on $SE(3)$ is:

$$\mathrm{I}\dot{\varpi} = ad^*_{\varpi}\mathrm{I}\varpi + f \tag{7}$$

where $ad^*_{\varpi} = (ad_{\varpi})^T$ is the dual map of ad_{ϖ}. The map $ad_{\varpi} : \mathbb{R}^6 \to \mathbb{R}^6$ is the adjoint operator which can be described as:

$$ad_{\varpi} = \begin{bmatrix} \hat{\Omega} & 0_{3\times 3} \\ \hat{V} & \hat{\Omega} \end{bmatrix} \in \mathbb{R}^{6\times 6} \tag{8}$$

$I \in \mathbb{R}^{6\times 6}$ is the inertial parameter related to the inertial matrix

$$J \in \mathbb{R}^{3\times 3}$$

and the mass $m \in \mathbb{R}_+$ of the spacecraft. I is described as:

$$I = \begin{bmatrix} J & 0_{3\times 3} \\ 0_{3\times 3} & mI_3 \end{bmatrix} \tag{9}$$

$\frac{1}{2}\varpi^T\mathrm{I}\varpi = \frac{1}{2}\Omega^T J\Omega + \frac{1}{2}mV^TV$ is designed to obtain the kinematic energy. $f \in \mathbb{R}^6$ is the resultant generalized force. Connecting the potential force with external disturbance, f can be described as:

$$f = u + d + f_g \tag{10}$$

where u is the designed input. $d \in \mathbb{R}^6$ is the generalized external disturbance result in model simplifications, parameter uncertainties and external interference. $f_g \in \mathbb{R}^6$ is the generalized potential force. Moreover, the formula (10) can be rewritten as:

$$f = \begin{bmatrix} f_\Omega \\ f_V \end{bmatrix} u = \begin{bmatrix} \tau \\ F \end{bmatrix} d = \begin{bmatrix} d_\Omega \\ d_V \end{bmatrix} f_g = \begin{bmatrix} M_g \\ F_g \end{bmatrix} \tag{11}$$

where $f_\Omega \in \mathbb{R}^3$ is the torque, $f_V \in \mathbb{R}^3$ is the resultant external force. $F \in \mathbb{R}^3$ and $\tau \in \mathbb{R}^3$ are input force and input torque, respectively. $d_V \in \mathbb{R}^3$ and $d_\Omega \in \mathbb{R}^3$ are the force and disturbance torque, respectively. $M_g \in \mathbb{R}^3$ and $F_g \in \mathbb{R}^3$ are the known moment and force caused by the potential forces, respectively.

Based on the formula (5), (8), and (10), formula (4) and (8) can be transformed as follow:

$$\begin{aligned} \dot{R} &= R\hat{\Omega} \\ \dot{p} &= RV \\ J\dot{\Omega} &= -\Omega \times J + \tau + d_\Omega + M_g \\ m\dot{V} &= -m\Omega \times V + F + d_V + F_g \end{aligned} \tag{12}$$

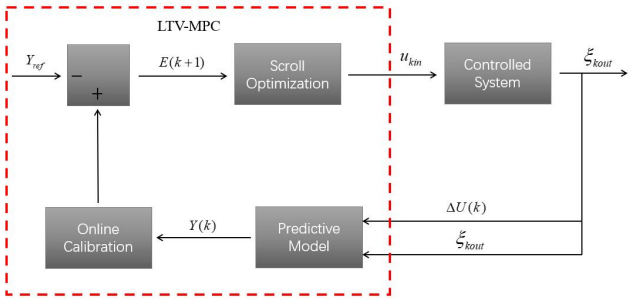

FIGURE 1. Linearization process of LTV.

B. LTV-MPC ALGORITHM ON $SE(3)$

The conventional MPC method is typically applicable to explicit discrete systems in Euclidean space $\mathbb{R}^n$. However, the dynamic equations on $SE(3)$ are implicit, making it challenging to obtain the optimal control directly using the MPC algorithm. To address this, we employ a method of approximate linearization for the state trajectory.

The approach involves applying a constant control input to the system and designing an LTV model predictive control algorithm based on the deviation between the system's state trajectory and the actual state values. This allows an approximate linear representation of the system. To elaborate on the linearization process, we consider the following steps:

One advantage of this method is that it does not require obtaining the state and control quantities of the desired trajectory in advance. This alleviates the need for accurate knowledge of the future trajectory and allows for a more flexible and adaptive control method.

1) The model of LTV-MPC

$\xi_r \in \Gamma, u_r \in \Omega$ are the state quantity and control quantity of the system at a certain operating point, respectively, which satisfy:

$$\begin{cases} \hat{\xi}_r(k+1) = f\left(\xi_r(k), u_r\right) \\ \hat{\xi}_r(0) = \xi_r \end{cases} \tag{13}$$

Using Taylor expansion at any point yields:

$$\begin{aligned} \dot{\xi} = f\left(\xi_r, u_r\right) &+ \left.\frac{\partial f}{\partial \xi}\right|_{\substack{\xi=\xi_r \\ u=u_r}} (\xi - \xi_r) \\ &+ \left.\frac{\partial f}{\partial u}\right|_{\substack{\xi=\xi_r \\ u=u_r}} (u - u_r) \end{aligned} \tag{14}$$

The formula (14) can also be rewritten as:

$$\dot{\xi} = f\left(\xi_r, u_r\right) + J_f(\xi)\left(\xi - \xi_r\right) + J_f(u)\left(u - u_r\right) \tag{15}$$

Let $J_f(\xi)$ be the Jacobian of f with respect to ξ, while let $J_f(u)$ be the Jacobian of f with respect to u. Based on the formula (14) and (15), the linearized linear time-varying equation can be obtained:

$$\dot{\xi}_d = A_d(t)\xi_d(t) + B_d(t)u_d(t) \tag{16}$$

where $\xi_d(t) = \xi - \xi_r$, $u_d(t) = u - u_r$, $A_d(t)$ and $B_d(t)$ are Jacobian matrix.

The obtained equation of state is continuous so it cannot be directly applied to model predictive control algorithm. Therefore, it is necessary to discretize this equation of state. The first-order difference quotient method is used for discretization in this paper, namely:

$$\begin{cases} A_d(k) = I + TA_d(k) \\ B_d(k) = TB_d(k) \end{cases} \tag{17}$$

where I denotes the principal diagonal matrix and T denotes the sampling interval.

According to the above formula, the state space system discretized by using linearization can be expressed as follow:

$$\xi_d(k+1) = A_d(k)\xi_d(k) + B_d(k)u_d(k) \tag{18}$$

The model predictive controller is designed according to the formula (18). Transforming control quantity $u_d(k)$ into control increment $\Delta u_d(k)$ yields:

$$\begin{cases} \tilde{\xi}_d(k+1 \mid k) = \tilde{A}_k\tilde{\xi}_d(k \mid k) + \tilde{B}_k\Delta u(k \mid k) \\ \eta(k \mid k) = \tilde{C}_k\tilde{\xi}_d(k \mid k) \end{cases} \tag{19}$$

where $\Delta u(k) = u_d(k) - u_d(k-1)$ and the coefficient matrix can be described as follow:

$$\begin{aligned} A &= \begin{bmatrix} A_d & B_d \\ 0_{m\times n} & I_m \end{bmatrix}, B = \begin{bmatrix} B_d \\ I_m \end{bmatrix}, C = \begin{bmatrix} C_d\, 0 \end{bmatrix} \\ \tilde{\xi}_d(k|k) &= \begin{bmatrix} \xi_d(k|k) \\ u_d(k-1|k) \end{bmatrix} \\ \Delta u(k) &= \begin{bmatrix} u_d(k) \\ u_d(k-1) \end{bmatrix} \end{aligned} \tag{20}$$

where $0_{m\times n}$ is null matrix with $m \times n$. I is the identity matrix in m dimensions. m is the dimensionality of the control variable and n is the dimensionality of the state variable.

In order to simplify the system computational complexity, we suppose:

$$\begin{aligned} A_k &= A_d(k), k = 1, \cdots, N_p \\ B_k &= B_d(k), k = 1, \cdots, N_c \\ C_k &= C_d(k), k = 1, \cdots, N_p \end{aligned} \tag{21}$$

Suppose N_p and N_c are the time-domain of prediction and the time-domain of control, respectively. The state variable and output in time domain system can be described as:

$$\begin{cases} \xi(k+N_p \mid k) = A^{N_p}\xi(k \mid k) + A^{N_p-1}B\Delta u(k \mid k) \\ + \cdots + A^{N_p-N_c-1}B\Delta u(k+N_c \mid k) \\ \eta(k+N_p \mid k) = CA^{N_p}\xi(k \mid k) + CA^{N_p-1}\Delta u(k \mid k) \\ + \cdots + CA^{N_p-N_c-1}\Delta u(k+N_c \mid k) \end{cases} \tag{22}$$

To make the relationship of the overall state space system clearer, the output of the system can be described as:

$$Y(k) = \Psi\tilde{\xi}(k \mid k) + \Theta\Delta U(k) \tag{23}$$

where $Y(k) = \begin{bmatrix} \eta(k+1 \mid k) \\ \cdots \\ \eta(k+N_c \mid k) \\ \cdots \\ \eta(k+N_p \mid k) \end{bmatrix}$, $\Psi = \begin{bmatrix} CA \\ \cdots \\ CA^{N_c} \\ \cdots \\ CA^{N_p} \end{bmatrix}$,

$\Delta U(t) = \begin{bmatrix} \Delta u(k \mid k) \\ \Delta u(k+1 \mid k) \\ \cdots \\ \Delta u(k+N_c \mid k) \end{bmatrix}$,

$$\Theta = \begin{bmatrix} CB & 0 & 0 & 0 \\ CAB & CB & 0 & 0 \\ \cdots & \cdots & \ddots & \cdots \\ CA^{N_c-1}B & CA^{N_c-2}B & \cdots & CB \\ CA^{N_c}B & CA^{N_c-1}B & \cdots & CAB \\ \vdots & \vdots & \ddots & \vdots \\ CA^{N_p-1}B & CA^{N_p-2}B & \cdots & CA^{N_p-N_c-1}B \end{bmatrix}.$$

Hence, it becomes evident that the system's state and output variables can be computed by iteratively cycling through the current state variables and control increments within the predictive time domain. This cyclic iterative process enables the realization of the prediction function within the model predictive controller.

2) Establishment of LTV-MPC model on $SE(3)$

To guarantee the spacecraft's attitude and position variables are same, the description of the spacecraft includes its position and velocity, which can be denoted as:

$$\begin{cases} p' = \dfrac{p}{p_m} \\ V' = \dfrac{V}{V_m} \end{cases} \tag{24}$$

where $p' \in \mathbb{R}^3$, $V' \in \mathbb{R}^3$ represent the normalized forms of the vector p and V, respectively. $p_m, V_m \in \mathbb{R}$ represent the normalized parameters of initial spatial coordinates and motion parameters error of spacecraft, respectively. Then the formula (12) can be rewritten as:

$$\begin{cases} \dot{R} = R\Omega^\wedge \\ \dot{p}' = \frac{V_m R V'}{p_m} \\ \dot{\Omega} = J^{-1}\left(-\boldsymbol{\Omega} \times J\Omega + \tau + d_\Omega\right) \\ \dot{V}' = \frac{-\boldsymbol{\Omega}\times m V_m V' + F + d_V}{m V_m} \end{cases} \tag{25}$$

The Lie group $SE(3)$ is a 6-dimensional nonlinear manifold with 16 elements and 10 nonlinear constraints. Traditional numerical integration methods, for example, Euler integration and Runge-Kutta integration, destroy the geometry of $SE(3)$. Therefore, the LGVI geometric integration method is used to obtain the nonlinear dynamic equation on $SE(3)$. Then, formula (14) can be rewritten as:

$$R_{k+1} = R_k f_k \tag{26}$$

$$f_k J_d - J_d f_k^T = h(J\boldsymbol{\Omega}_k)^\wedge \tag{27}$$

$$p'_{k+1} = p'_k + \frac{hV_m}{p_m} R_k V'_k \tag{28}$$

$$J\boldsymbol{\Omega}_{k+1} = f_k^T J\boldsymbol{\Omega}_k + h\tau_k \tag{29}$$

$$mV'_{k+1} = f_k^T mV'_k + \frac{h}{V_m}F_k \tag{30}$$

where, $J_d \in \mathbb{R}^{3\times3}$ is defined as $J_d = \frac{1}{2}tr(J)I - J$. $R_k \in SO(3), \Omega_k \in \mathbb{R}^3$ are the attitude and angular velocity of spacecraft at time $k, k = 1, 2, ..., N-1$, respectively. $p'_k \in \mathbb{R}^3$, $V'_k \in \mathbb{R}^3$ are the position and translational velocity of the spacecraft at time k . $f_k \in SO(3)$ is the group variable at attitude R_k . $\tau_k \in \mathbb{R}^3, F_k \in \mathbb{R}^3$ represent the input torque and force of external input, respectively. h is the integral step.

To update the current state variable $(R_k, \Omega_k, p'_k, V'_k)$ and input variable (τ_k, F_k) , first, the equation (27) is used to update f_k; second, (26) and (29) are solved to update R_{k+1}, Ω_{k+1}. (28) and (30) are solved to update p'_{k+1}, V'_{k+1}. Then, according to the designed control law and $(R_{k+1}, \Omega_{k+1}, p'_{k+1}, V'_{k+1})$ to calculate input variable (τ_{k+1}, F_{k+1}).

Design the state vector X_k of the discrete dynamic system, output vector Y_k and input vector U_k as:

$$\begin{cases} X_k = \begin{bmatrix} R_k & {p'}_k & \Omega_k & {V'}_k \end{bmatrix} \\ Y_k = \begin{bmatrix} R_k & {p'}_k & \Omega_k & {V'}_k \end{bmatrix} \\ U_k = \begin{bmatrix} \tau_k & {F'}_k \end{bmatrix} \end{cases} \tag{31}$$

where $F'_k = \frac{F_k}{V_m}$ is the normalized control force.

3) The solution of implicit equation

This section will introduce a method to find the solution to the implicit equation. The traditional method can only obtain the approximate solution by numerical method. As the equation (27) is nonlinear, make

$$M_k = h(J\boldsymbol{\Omega}_k)^\wedge \tag{32}$$

the (27) can be rewritten as:

$$f_k J_d - J_d f_k^T = M_k \tag{33}$$

Then

$$f_k = (M_k/2 + S_k)\, {J_d}^{-1} \tag{34}$$

We know that S_k a solution to the algebraic Riccati equation [1]. If and only if ${J_d}^2 + M_k^2/4$ is positive semi-definite, namely:

$${J_d}^2 + M_k^2/4 \geqslant 0 \tag{35}$$

4) Taylor expansion on $SE(3)$

According to the formula (26)-(30), the implicit discrete dynamic equation on $SE(3)$ is mainly obtained by $R_k \in SO(3)$. Based on the reference [19], [20], the infinitesimal variable $dR \in T_R SO(3)$ on $R \in SO(3)$ can be described as:

$$dR = R\hat{\eta} \tag{36}$$

where $\eta \in \mathbb{R}^3, \hat{\eta} \in so(3)$. According to the left invariant principle of Lie groups, dR can be equivalent to η. By invoking [19] and [20], taking the derivative of η yields:

$$\dot{\eta} = d\Omega - \hat{\Omega}\eta \tag{37}$$

The infinitesimal variable of $\dot{p'}, \dot{\Omega}$ and $\dot{V'}$ can be described by variable principle

$$d\dot{p'} = \frac{V_m}{p_m}R\hat{\eta}V' + \frac{V_m}{p_m}Rd\dot{V'} \tag{38}$$

$$d\dot{\Omega} = J^{-1}((J\Omega)^\wedge - \hat{\Omega}J)d\Omega + J^{-1}d\tau \tag{39}$$

$$d\dot{V'} = \hat{V'}d\Omega - \hat{\Omega}dV' + \frac{1}{m}dF' \tag{40}$$

As dR can be equivalent to η, the state variable in the formula (31) can be described as:

$$dX = \begin{bmatrix} \eta \\ dp' \\ d\Omega \\ dV' \end{bmatrix} \in \mathbb{R}^{12} \tag{41}$$

$$dY = \begin{bmatrix} \eta \\ dp' \\ d\Omega \\ dV' \end{bmatrix} \in \mathbb{R}^{12} \tag{42}$$

$$dU = \begin{bmatrix} d\tau \\ dF' \end{bmatrix} \in \mathbb{R}^6 \tag{43}$$

According to the formula (37)-(40), the derivative of $d\dot{X}$ with respect to time, dX can be rewritten as:

$$d\dot{X} = \begin{bmatrix} -\hat{\Omega} & 0 & I & 0 \\ -\frac{V_m}{p_m}R\hat{V'} & 0 & 0 & \frac{V_m}{p_m}R \\ 0 & 0 & J^{-1}((J\Omega)^\wedge - \hat{\Omega}J) & 0 \\ 0 & 0 & \hat{V'} & -\hat{\Omega} \end{bmatrix} dX + \begin{bmatrix} 0 & 0 \\ 0 & 0 \\ J^{-1} & 0 \\ 0 & \frac{1}{m}I \end{bmatrix} dU \tag{44}$$

where this formula is a continuous dynamic system with the state variable dX and the input variable dU. Moreover, this formula is a continuous dynamic system with the state variation dX and the input variation dU. To simplify the design and application of MPC method, formula (25) should be transformed into the form of discrete dynamic. According to Euler integral, (25) can be rewritten as:

$$dX_{k+1} = dX_k + h(d\dot{X})_k = A'_k dX_k + B'_k dU_k \tag{45}$$

where $(d\dot{X})_k$ is the discrete variation sampled at time k. Matrices $A'_k \in \mathbb{R}^{12\times12}$ and $B'_k \in \mathbb{R}^{12\times6}$ are described as follows:

$$\begin{cases} A_k = \begin{bmatrix} I - h\hat{\boldsymbol{\Omega}}_k & \mathbf{0} & hI & \mathbf{0} \\ -\frac{hV_m}{p_m}R_k\hat{V}'_k & I & \mathbf{0} & \frac{hV_m}{p_m}R_k \\ \mathbf{0} & \mathbf{0} & K & 0 \\ 0 & 0 & h\hat{V}'_k & I - h\hat{\boldsymbol{\Omega}}_k \end{bmatrix} \\ B_k = \begin{bmatrix} 0 & 0 \\ 0 & 0 \\ hJ^{-1} & 0 \\ 0 & \frac{h}{m}I \end{bmatrix} \end{cases} \tag{46}$$

where $K = I - hJ^{-1}\left((J\boldsymbol{\Omega}_k)^{\wedge} - \hat{\boldsymbol{\Omega}}_k J\right)$.

As the state variable dX and dU are infinitesimal variables. In the formula (18), $\xi_d(k)$ represents the variable in the output produced by the correction, and $u_d(k)$ represents the correction of the control quantity. Therefore, by considering small quantity approximation, dX and dU are equal to $\xi_d(k)$ and $u_d(k)$, respectively. Namely, $dX = \xi_d(k)$, $dU = u_d(k)$. Then the Matrices $A'_k \in \mathbb{R}^{12\times12}$ and $B'_k \in \mathbb{R}^{12\times6}$ can be used in (18). $\xi_d(k)$ and $u_d(k)$ can be described as:

$$\xi_d(k) = \begin{bmatrix} \varsigma \\ p' \\ \Omega \\ V' \end{bmatrix} \in \mathbb{R}^{12} \tag{47}$$

where $\varsigma^{\wedge} = \log R$

Therefore, the LTV-MPC algorithm (19) can be used on $SE(3)$.

III. CONTROLLER DESIGN

A. TRAJECTORY TRACKING

1) Trajectory tracking controller design.

To achieve trajectory tracking, the objective function is considered as:

$$\begin{cases} J(\xi(k), u(k-1), \Delta U(k)) = \sum_{i=1}^{N_p} \eta\left(k+i\,|k\right) - \\ \quad \eta_r\left(k+i\,|k\right)_Q^2 + \sum_{i=1}^{N_c-1} \|\Delta u(k+i\,|k)\|_R^2 \end{cases} \tag{48}$$

Although the function (48) has higher tracking accuracy and can predict the control sequence for the next period, the prediction model based on the spacecraft dynamics model is complex and variable. Therefore, the optimization objective needs to be treated by adding relaxation factor to the objective function, which is expressed as:

$$\begin{aligned} &J(\xi(k), u(k-1), \Delta U(k)) \\ &= \sum_{i=1}^{N_{p-1}} \|\eta(k+i\,|k) - \eta_r(k+i\,|k)\|_Q^2 \\ &+ \sum_{i=1}^{N_c-1} \|\Delta u(k+i\,|k)\|_R^2 \\ &+ \rho\varepsilon^2 + \eta(k+N_p\,|k)^T P \eta(k+N_p\,|k) \end{aligned} \tag{49}$$

where ρ is the weight coefficient, ε is the relaxation factor.

The formula (49) can be written as:

$$\begin{aligned} J(X(k), u(k-1), U(k)) = [\Delta U(k), \varepsilon]^T H \left[\Delta U(k)^T, \varepsilon\right] \\ + G\left[\Delta U(k), \varepsilon\right] + P_d \end{aligned} \tag{50}$$

where $H = \begin{bmatrix} \Theta^T Q_e \Theta & 0 \\ 0 & \rho \end{bmatrix}$, $P_d = \tilde{\xi}(k\,|k)^T(\Psi^T Q_e \Psi + P)\tilde{\xi}(k\,|k)$ and $G = \begin{bmatrix} 2E(k)Q_e\Theta & 0 \end{bmatrix}$.

The output deviation in system time-domain prediction is described as:

$$\begin{cases} E(k) = \Psi X(k\,|k) - Y_r(k) \\ Y_r(k) = [\eta_r(k+1\,|t), ..., \eta_r(k+N_p\,|k)]^T \end{cases} \tag{51}$$

In the case of quadratic programming solving the minimum, the constant term does not affect the results. Therefore, the quadratic programming form of the controller specialized in trajectory tracking is described as:

$$\begin{aligned} &\min_{\Delta U(k)} J(X(k), u(k-1), \Delta U(k)) \\ &= \frac{1}{2}\left[\Delta U(k)^T, \varepsilon\right]^T 2H \left[\Delta U(k)^T, \varepsilon\right] \\ &+ G\left[\Delta U(k)^T, \varepsilon\right] \end{aligned} \tag{52}$$

2) Feedback mechanism of controller design

As section 3.1 analyzes, in the case of the linear constraint is satisfied, by obtaining the optimal control quantity $\Delta U(k)$, the objective function can be minimized. Based on the controller for the kinetic model, when the solution has been completed in each control iteration, a series of relaxation factors and increments of control input in the control time domain N_c are obtained

$$\begin{bmatrix} \Delta u^{\circ}(k\,|k) \\ \Delta u^{\circ}(k+1\,|k) \\ \cdots \\ \Delta u^{\circ}(k+N_c\,|k) \\ \varepsilon \end{bmatrix} \tag{53}$$

The first element in the optimal control sequence is taken as the actual control input increment, which can be described as:

$$u(k) = u(k-1) + \Delta u^{\circ}(k \mid k) \tag{54}$$

After entering the next control cycle, according to the state quantity obtained at the current moment and the input at the previous moment, the $SE(3)$ fully actuated spacecraft model is updated. Then the objective function is solved and the optimal control increment sequence is obtained until the control of desired trajectory tracking is achieved.

B. OBSTACLE AVOIDANCE

1) Obstacle avoidance statement

In this section, the obstacle avoidance scheme in this paper is introduced. In order to solve the problem of needing to solve an optimization proposition in each rolling time domain of MPC, the MPC algorithm is used for single-layer obstacle avoidance control. As the spacecraft has multiple constraints, if the information about the obstacle is added to the optimization proposition as a constraint condition, it may cause unsolvable problems of the optimization objective. To solve the optimization proposition by using the quadratic programming method, obstacle information is added to the optimization proposition in the form of a penalty function. Then the original penalty function is approximated near the

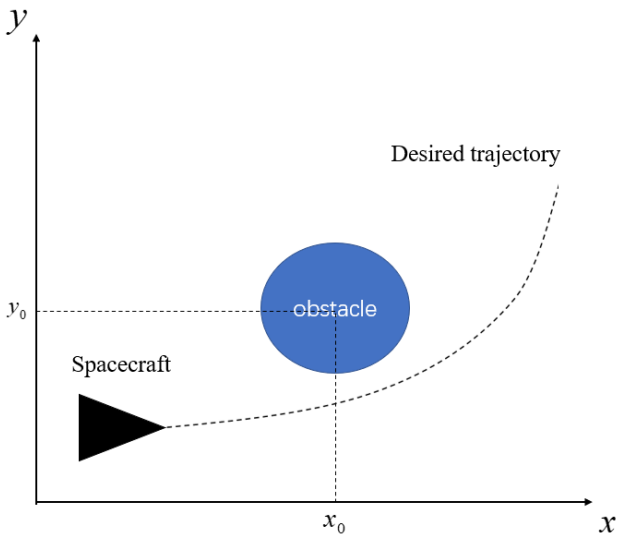

FIGURE 2. Obstacle avoidance diagram.

nominal locus point, and Taylor expansion is used for the obstacle avoidance algorithm of the spacecraft.

As Fig. 2 described, (x_0, y_0, z_0) is the center position of the obstacle in the inertial reference system. In this part, we suppose that there is a desired trajectory in the space. When the full actuated spacecraft is tracking the desired trajectory, an obstacle appeared on the trajectory. The spacecraft avoid obstacles without changing the desired trajectory. When obstacle avoidance is complete, the spacecraft return to the desired trajectory.

2) Construction of obstacle avoidance function

According to the penalty function methods for dealing with constraints in numerical optimization. The obstacle avoidance penalty function is constructed as follow:

$$\begin{aligned} J_{\mathrm{Obs}} &= J(x, y, z) \\ &= S_{Obs} Ln((x - x_0)^2 + (y - y_0)^2 + (z - z_0)^2 + \xi) \end{aligned} \tag{55}$$

where S_{Obs} is the weight function of obstacle avoidance, Ln is a logarithmic function with a natural base. (x_0, y_0, z_0) is the center position of the obstacle. ξ is the maximum value, which is expressed as:

$$\sum_{i=1}^{N_p} J_{\mathrm{Obs}}(X_{obs}(k+1), Y_{obs}(k+1), Z_{obs}(k+1)) \tag{56}$$

3) Second order approximation based on Taylor expansion

In this section, the Taylor formula is used to expand the obstacle avoidance function in the vicinity of the nominal trajectory point. As the quadratic programming proposition at most the order of the proposition solution is quadratic, the obstacle avoidance function is expanded into the second order.

Suppose the current is time k, expanding the obstacle avoidance function into the second order at the vicinity of the nominal trajectory point yields:

$$\begin{aligned} &J_{tarlor}(X(k), Y(k), Z(k)) \\ &= J(X_k, Y_k, Z_k) + \begin{bmatrix} J_x & J_y & J_z \end{bmatrix} \begin{bmatrix} (X - X_k) \\ (Y - Y_k) \\ (Z - Z_k) \end{bmatrix} + \\ &\frac{1}{2}\left[(X - X_k)(Y - Y_k)(Z - Z_k)\right] \begin{bmatrix} J_{11} & J_{12} & J_{13} \\ J_{21} & J_{22} & J_{23} \\ J_{31} & J_{32} & J_{33} \end{bmatrix} \\ &\begin{bmatrix} (X - X_k) \\ (Y - Y_k) \\ (Z - Z_k) \end{bmatrix} \end{aligned} \tag{57}$$

where (X_k, Y_k, Z_k) represents the space coordinates of the spacecraft.

$$J_x = \frac{2S_{obs}(X_k - X_0)}{\left[(X_k - X_0)^2 + (Y_k - Y_0)^2 + (Z_k - Z_0)^2 + \zeta\right]}$$

$$J_{11} = -\frac{4S_{obs}(X_t - X_0)^2}{\left[(X_k - x_0)^2 + (Y_k - Y_0)^2 + (Z_k - Z_0)^2 + \zeta\right]^2} + \frac{2S_{obs}}{\left[(X_k - X_0)^2 + (Y_k - Y_0)^2 + (Z_k - Z_0)^2 + \zeta\right]}$$

$$J_{12} = -\frac{4S_{obs}(X_k - X_0)(Y_k - Y_0)}{\left[(X_k - X_0)^2 + (Y_k - Y_0)^2 + (Z_k - Z_0)^2 + \zeta\right]^2}$$

Moreover, the remaining characterization parameters possess identical structures and can be readily determined.

Using Taylor expansion on the rolling optimization proposition yields:

$$\begin{aligned} &\min \sum_{i=1}^{N_p} J_{Obs}\left(X(k+i), Y(k+i), Z(k+i)\right) \\ &= \min \sum_{i=1}^{N_p} D_J \bar{X}(k+i|k) + \frac{1}{2}\bar{X}(k+i|k)^T Q_J \bar{X}(k+i|k) \\ &= \min \bar{D}_J Y(k) + \frac{1}{2} Y(k)^T \bar{Q}_J Y(k) \\ &= \min \sum_{i=1}^{N_p} J_{\mathrm{Obs}}(X(k+i), Y(k+i), Z(k+i)) \\ &= \min \frac{1}{2}\Delta U(k)^T \left(\Theta^T \bar{Q}_J \Theta\right) \Delta U(k) \\ &+ \left(\tilde{X}(k \mid k)^T \Psi^T \bar{Q}_J + \bar{D}_J\right) \Theta \Delta U(k) \\ &Y(k) = \begin{bmatrix} \eta(k+1 \mid k) \\ \cdots \\ \eta(k+N_c \mid k) \\ \cdots \\ \eta(k+N_p \mid k) \end{bmatrix} \end{aligned} \tag{58}$$

where $Y(k) = \Psi \tilde{X}(k \mid k) + \Theta \Delta U(k)$

$$D_J = \begin{bmatrix} 0 & 0 & 0 & J_x & J_y & J_z & 0 & 0 & 0 & 0 & 0 & 0 \end{bmatrix}$$

$$Q_j = \begin{bmatrix} D_x \\ D_y \\ D_z \end{bmatrix}^T \begin{bmatrix} J_{11} & J_{12} & J_{13} \\ J_{21} & J_{22} & J_{23} \\ J_{31} & J_{32} & J_{33} \end{bmatrix} \begin{bmatrix} D_x \\ D_y \\ D_z \end{bmatrix}$$

$$D_x = \begin{bmatrix} 0 & 0 & 0 & 1 & 0 & 0 & 0 & 0 & 0 & 0 & 0 & 0 \end{bmatrix}$$

$$D_y = \begin{bmatrix} 0 & 0 & 0 & 0 & 1 & 0 & 0 & 0 & 0 & 0 & 0 & 0 \end{bmatrix}$$

$$D_z = \begin{bmatrix} 0 & 0 & 0 & 0 & 0 & 1 & 0 & 0 & 0 & 0 & 0 & 0 \end{bmatrix}$$
$$\bar{D}_J = [D_J D_J \ \cdots D_J \, D_J]$$
$$\bar{Q}_J = \begin{bmatrix} Q_J & & & & \\ & Q_J & & & \\ & & Q_J & & \\ & & & \ddots & \\ & & & & Q_J \end{bmatrix}$$

Then, by transforming the obstacle avoidance penalty function into a quadratic programming form can add it into the objective function to do the optimal solution.

4) Obstacle avoidance design in multi-obstacle situations

According to the QP quadratic form of trajectory tracking controller, by combining the two parts of quadratic programming, the trajectory tracking algorithm with obstacles can be obtained. If there are multiple obstacles in the space, the obstacle information can be successively added into the optimized objective function.

Suppose there are two obstacles in the space, the quadratic programming function can be described as:

$$\begin{aligned} &\min_{\Delta U(k)} J(\tilde{X}(k), u(k-1), \Delta U(k)) \\ &= \frac{1}{2}\left[\Delta U(k)^T, \varepsilon\right]^T W \left[\Delta U(k)^T, \varepsilon\right] \\ &+ M \left[\Delta U(k)^T, \varepsilon\right] \end{aligned} \tag{59}$$

where

$$W = \begin{bmatrix} 2\Theta^T Q_e \Theta + 2R_e + \Theta^T \bar{Q}_{J1} \Theta + \Theta^T \bar{Q}_{J2} \Theta & 0 \\ 0 & \rho \end{bmatrix}$$
$$M = \begin{bmatrix} 2E(k) Q_e \Theta + \tilde{X}(k \mid k)^T \Psi^T \bar{Q}_{J1} + \\ \bar{D}_{J1} + \tilde{X}(k \mid k)^T \Psi^T \bar{Q}_{J2} + \bar{D}_{J2} \\ 0 \end{bmatrix}^T$$
$$\Delta U(k) = \begin{bmatrix} \Delta u(k \mid k) \\ \Delta u(k+1 \mid k) \\ \cdots \\ \Delta u\left(k + N_c \mid k\right) \end{bmatrix}$$

The output deviation in the time domain of the system prediction is described as:

$$\begin{cases} E(k) = \Psi \tilde{X}(k \mid k) - Y_r(k) \\ Y_r(k) = [\eta_r(k+1 \mid t), \cdots, \eta_r\left(k + N_p \mid k\right)]^T \end{cases} \tag{60}$$

where $\bar{Q}_{J1}$ and $\bar{D}_{J1}$ are the information of the first obstacle, $\bar{Q}_{J2}$ and $\bar{D}_{J2}$ are the information of the second obstacle.

C. ERROR DESCRIPTION

Construct group error as follow:

$$g_e\left(g, g_d\right) = g \otimes {g_d}^{-1} \triangleq \begin{bmatrix} {R_d}^T R & p - p_d \\ 0_{1\times 3} & 1 \end{bmatrix} \tag{61}$$

where $g_d \in SE(3)$ is the desired configuration of the spacecraft. $\varpi_d \in \mathbb{R}^6$ is the velocity in the generalized space of the spacecraft. $R_d \in SO(3)$, $p_d \in \mathbb{R}^3$ are the desired attitude and desired position of the spacecraft, respectively. $\Omega_d \in \mathbb{R}^3$ is the angular velocity of the spacecraft. $V_d \in \mathbb{R}^3$ translational velocity of the spacecraft. In addition, I_4 is the zero element of the $SE(3)$. $g_e = I_4$ exists when the equation $g = g_d$ is satisfied.

According to the desired configuration, generalized velocity signal (g_d, ϖ_d) on $SE(3)$, the configuration and generalized velocity of the spacecraft at the present time (g, ϖ), the configuration error function ϕ_g, configuration error vector e_g and generalized speed vector e_ϖ can be described as follow:

$$\begin{cases} \phi_g = \phi_R + \phi_p \\ \phi_R = 2 - \sqrt{1 + tr\left(R_d^T R\right)} \\ \phi_p = \frac{1}{2} p - {p_d}^2 \end{cases} \tag{62}$$

$$\begin{cases} e_g = \begin{bmatrix} e_R \\ e_p \end{bmatrix} \\ e_R = \dfrac{1}{2\sqrt{1 + tr\left({R_d}^T R\right)}} \left({R_d}^T R - R^T R_d\right)^\wedge \\ e_p = R^T \left(p - p_d\right) \end{cases} \tag{63}$$

$$\begin{cases} e_\varpi = \begin{bmatrix} e_\Omega \\ e_V \end{bmatrix} \\ e_\Omega = \Omega - R^T R_d \Omega_d \\ e_\Omega = V - R^T R_d V_d \end{cases} \tag{64}$$

In the formula (61), ϕ_R is the attitude deviation function defined on manifold SO(3). ϕ_p is the position deviation function, which describes the absolute distance of the current position and the desired position of the spacecraft. In the formula (62), e_g is the configuration error vector on $SE(3)$. e_R, e_p are the attitude deviation vector and position deviation vector between current and desired configuration. In the formula (63), e_Ω and e_V are angular velocity deviation vector and translational velocity error vector of spacecraft, respectively. e_ϖ is the generalized velocity deviation vector, which can also be expressed as:

$$e_\varpi = \varpi - \alpha \tag{65}$$

where

$$\alpha = \begin{bmatrix} R^T R_d \Omega_d \\ R^T R_d V_d \end{bmatrix} \tag{66}$$

D. PROOF OF FEASIBILITY AND STABILITY OF LTV-MPC

Theorem 1 At the initial time $k = 0$, if the equation (54) was feasible, it will be feasible at any time in the future.

Proof The feasible solution of the optical problem at the time k=0 can be described as

$$\Delta U^\circ(k) = \begin{bmatrix} \Delta u^\circ(k \mid k) \\ \Delta u^\circ(k+1 \mid k) \\ \cdots \\ \Delta u^\circ\left(k + N_{c-1} \mid k\right) \end{bmatrix} \tag{67}$$

The predictive state is:

$$Y^{\circ}(k+1)=\begin{bmatrix}\eta^{\circ}(k+1\mid k)\\ \cdots\\ \eta^{\circ}\left(k+N_c\mid k\right)\\ \cdots\\ \eta^{\circ}\left(k+N_{p-1}\mid k\right)\\ 0\end{bmatrix} \tag{68}$$

where, because of the terminal punishment item, the terminal state of (67) is set to 0. At the time $k+1$, the feasible solution of the control law is substituted into the updated state, then the control of the next moment is described as:

$$\begin{aligned}\Delta U(k+1)&=\begin{bmatrix}\Delta u(k+1\mid k+1)\\ \Delta u(k+2\mid k+1)\\ \cdots\\ \Delta u\left(k+N_c+1\mid k+1\right)\end{bmatrix}\\ &=\begin{bmatrix}\Delta u^{\circ}(k+1\mid k+1)\\ \Delta u^{\circ}(k+2\mid k+1)\\ \cdots\\ \Delta u^{\circ}\left(k+N_c\mid k+1\right)\\ 0\end{bmatrix}\end{aligned} \tag{69}$$

Then the predictive state of it can be expressed as:

$$\begin{aligned}Y(k+2)&=\begin{bmatrix}\eta(k+2\mid k+1)\\ \eta(k+3\mid k+1)\\ \cdots\\ \eta\left(k+N_c\mid k+1\right)\\ \cdots\\ \eta\left(k+N_p-1\mid k+1\right)\\ \eta\left(k+N_p\mid k+1\right)\end{bmatrix}\\ &=\begin{bmatrix}\eta^{\circ}(k+2\mid k+1)\\ \eta^{\circ}(k+3\mid k+1)\\ \cdots\\ \\ \eta^{\circ}\left(k+N_{p-1}\mid k+1\right)\\ 0\\ 0\end{bmatrix}\end{aligned} \tag{70}$$

Therefore, a solution U which satisfied terminal constraints exists at least. Namely, if a feasible optimal solution exists at initial time, it is feasible at any time in the future.

Theorem 2 By using LTV-MPC, the tracking error closed-loop system has uniform asymptotic stability.

Proof Select the current optimal function $J^*(k)$ at the time k as the Lyapunov function:

$$\begin{aligned}V(k)&=J^*(k)\\ &=\sum_{i=1}^{N_{p-1}}\left\|\eta(k+i\mid k)-\eta_r(k+i\mid k)\right\|_Q^2\\ &+\sum_{i=1}^{N_c-1}\left\|\Delta u(k+i\mid k)\right\|_R^2+\rho\varepsilon^2\\ &+\eta(k+N_p\mid k)^T P\eta(k+N_p\mid k)\end{aligned} \tag{71}$$

where $V(0)=0$ and $V(k)>0$, namely, the control quantity and state quantity are not equal to 0. $V(k)\geqslant\left\|\eta(k|k)-\eta_r(k|k)\right\|_Q^2$ and there exists $\delta>0$ such that $V(k)\leqslant\delta\left\|\eta(k|k)-\eta_r(k|k)\right\|_Q^2$.

Then at the time $k+1$, the value of the cost function is:

$$\begin{aligned}J(k+1)=&J^*(k)-\left\|\eta^*(k\,|k)-\eta_r(k\,|k)\right\|_Q^2-\\ &\left\|\Delta u^*(k\,|k)\right\|_R^2\end{aligned} \tag{72}$$

Subtracting (72) into (71) yields:

$$\begin{aligned}V(k+1)-V(k)&=J^*(k+1)-J^*(k)\\ &\leqslant J^{\bullet}(k+1)-J^*(k)\\ &\leqslant-\left\|\eta^*(k\mid k)-\eta_r(k\mid k)_Q^2\right\|-\\ &\left\|\Delta u^*(k\mid k)\right\|_R^2\\ &\leqslant 0\end{aligned} \tag{73}$$

where $J^*(k+1)$ is the optimal solution of the objective solution at $k+1$ time and this optimal solution is considered as Lyapunov function at $k+1$ time. $J^{\bullet}(k+1)$ is the feasible solution (not optimal solution) at $k+1$ time. As the feasible solution is greater than the optimal solution in equation (73), the first inequality is feasible. Then, $V(k)$ is monotonic non increasing function can be obtained. According to equations (71)-(73), the LTV-MPC linearized closed-loop system satisfies the asymptotically uniform stability condition.

Therefore, the Lyapunov function $V(k)$ is monotonic decrement.

IV. SIMULATION

A. SETTINGS

In this section, some parameters used in the simulation are shown. First, the parameters of the spacecraft described in this paper are shown as follow:

TABLE 1. Parameters.

Parameter	Parameter
$J=diag\left(\begin{bmatrix}4.85 & 5.10 & 4.76\end{bmatrix}\right)kg\cdot m^2$	$F=\begin{bmatrix}0 & 0 & 0\end{bmatrix}^T N$
$x=\begin{bmatrix}-2.492 & 1.486 & -1.121\end{bmatrix}rad$	$p_1=\begin{bmatrix}5 & 1 & 3\end{bmatrix}^T m$
$\omega=\begin{bmatrix}0 & 0 & 0\end{bmatrix}^T rad/s$	$h=1$
$V=\begin{bmatrix}0 & 0 & 0\end{bmatrix}^T m/s$	$p_m=8$
$\tau=\begin{bmatrix}0 & 0 & 0\end{bmatrix}^T Nm$	$V_m=8$
$m=56.7kg$	

Where $\begin{bmatrix}5 & 5 & 5\end{bmatrix}^T$ is the initial position of the spacecraft. Moreover,
$Q=diag\left([20,20,20,1500,1500,2000,1,1,1,1,1,1]\right)$, $R=diag\left([1,1,1,10,10,10]\right)$ and $\rho=500000$ are the obstacle avoidance weight matrices of the spacecraft. However, the weight matrices are adjusted to 0 if there are no obstacles on the trajectory of the spacecraft.

Then, to show the effectiveness of the obstruct avoidance of the spacecraft, the parameters of the four obstacles are shown as follow:

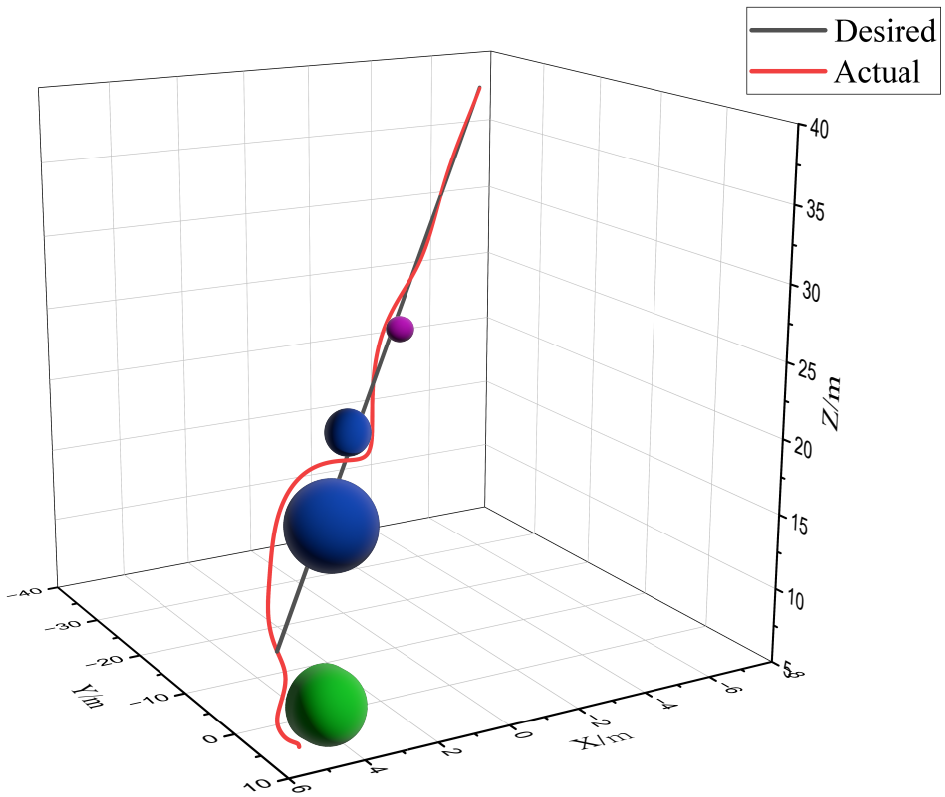

FIGURE 3. Actual trajectory and desired trajectory diagram.

TABLE 2. Parameters.

Obstacle 1	Obstacle 2	Obstacle 3	Obstacle 4
$S_{Obs1} = 120$ $x_1 = 5m$ $y_1 = 2m$ $z_1 = 6m$ $\zeta_1 = 0.5$	$S_{Obs2} = 200$ $x_2 = 3m$ $y_2 = -5m$ $z_2 = 15m$ $\zeta_2 = 0.7$	$S_{Obs3} = 80$ $x_3 = 1m$ $y_3 = -12m$ $z_3 = 20m$ $\zeta_3 = 0.12$	$S_{Obs4} = 10$ $x_4 = -2m$ $y_4 = 18m$ $z_4 = 28m$ $\zeta_4 = 0.05$

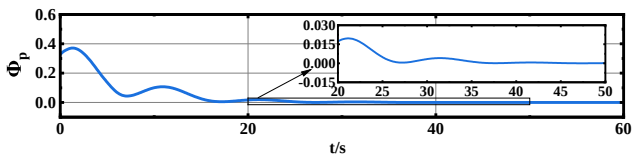

FIGURE 4. Position error function diagram.

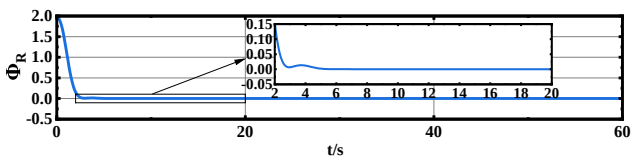

FIGURE 5. Attitude error function diagram.

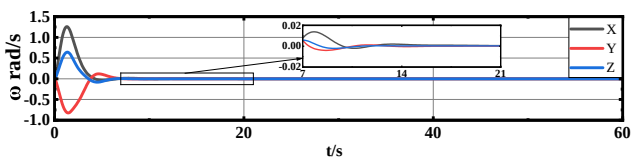

FIGURE 6. Angular velocity error vector diagram.

B. SIMULATION RESULTS

In this section, to demonstrate the effectiveness and superiority of the proposed control scheme, the simulation results are introduced.

From Fig. 3, the obstacle on the approaching trajectory is green, the two obstacles on the desired trajectory are blue and the obstacle deviate from the desired trajectory is purple, we can obtain the spacecraft can track the desired trajectory and complete the obstacle avoidance task. The performance of obstacle avoidance is different when the obstacle avoidance weight varies. As the obstacle avoidance weight is set larger, the performance of obstacle avoidance is better.

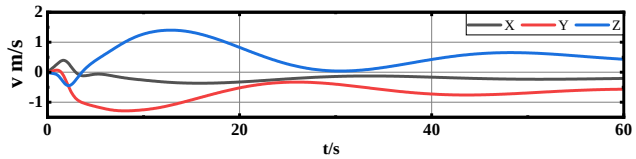

FIGURE 7. Velocity error vector diagram.

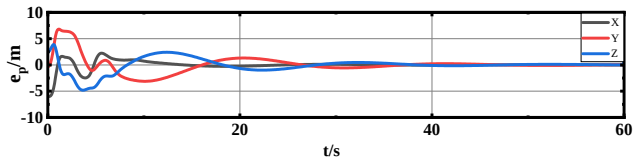

FIGURE 8. Position error vector.

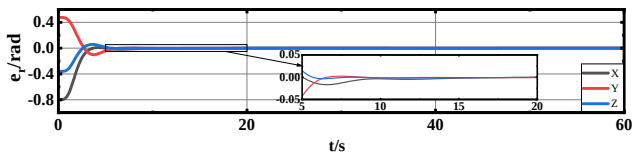

FIGURE 9. Attitude error vector.

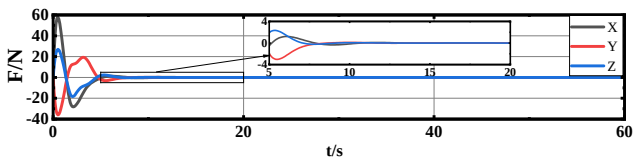

FIGURE 10. Control force diagram.

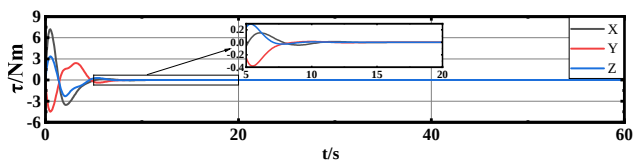

FIGURE 11. Control torque diagram.

Fig. 4 and Fig. 5 show the configuration error function ϕ_g and attitude error function ϕ_R under the LTV-MPC control algorithm, which represents the absolute distance between the actual position and the expected position of the spacecraft, as well as the current attitude and the expected attitude. As can be seen in Fig. 4 and Fig. 5 the attitude error function converges to 0 within $6s$. The position error function reaches within 0.1 before $25s$. These illustrate that the spacecraft can track the desired trajectory and attitude effectively under the proposed method.

Fig. 6 and Fig. 9 show attitude error vector e_R and angular velocity error vector e_ω of the attitude subsystem of a fully driven spacecraft on manifold $SE(3)$. From Fig. 6 and Fig. 9 that attitude error vector e_R and angular velocity error vector e_ω based on $SE(3)$ can both converge to 0 asymptotically under the LTV-MPC control scheme. Moreover, $\|e_R\|$, $\|e_\Omega\| \leqslant 10^{-3}$ and control scheme in this paper has high robustness.

Fig. 7 illustrates the velocity error vector e_V and Fig. 8 illustrates the position error e_P under the LTV-MPC algorithm based on $SE(3)$. It can be seen that the velocity error vector e_V and the position error e_P can converge to 0 in finite time under the control scheme proposed in this paper.

Fig. 10 and Fig. 11 demonstrate the control torque τ and control force F obtained by the LTV-MPC algorithm. It can be seen that the control torque τ and the control force F can converge to 0 within $10s$. This simulation result indicates that the control scheme in this paper has fast convergence velocity and high control accuracy. In addition, the corresponding control input is stable without flutter, so it can be directly applied to engineering practice.

According to the description illustrated above, it can be seen that the full drive spacecraft with 6 - DOF can achieve fast obstacle avoidance and high precision trajectory tracking, which can be used in space mission effectively.

V. CONCLUSION

This paper introduces a fully driven spacecraft trajectory tracking controller that utilizes a linear time-varying model predictive control approach. The controller takes into account the potential presence of space obstacles during the spacecraft's mission. First, an integrated $SE(3)$ attitude trajectory model is established for the fully driven spacecraft. The dynamic error model for the trajectory tracking system is then developed using linear time-varying theory. The non-linear tracking error system is addressed through a linearization method, and the optimization function is augmented with an obstacle avoidance function and relaxation factor to ensure feasible solutions. The effectiveness of the proposed controller is evaluated through numerical simulations. The results illustrate the controller accurately and rapidly tracks the desired trajectory within a finite time. Both attitude and position tracking errors achieve a high accuracy of 10^{-8}, and the controller exhibits robustness. Additionally, the controller appropriately avoids space obstacles, ensuring mission safety. Hence, the proposed controller is suitable for various complex working environments and task requirements. However, this paper consider the fully-actuated spacecraft. In the future research, we will study and analyze the characteristics of actuators and communication delay in the integrated control of under-actuated spacecraft.

REFERENCES

[1] Gong K, Liao Y, Wang Y. Adaptive fixed-time terminal sliding mode control on SE (3) for coupled spacecraft tracking maneuver[J]. International Journal of Aerospace Engineering, 2020, 2020: 1-15.

[2] Shirobokov M, Trofimov S, Ovchinnikov M. Survey of machine learning techniques in spacecraft control design[J]. Acta Astronautica, 2021, 186: 87-97.

[3] Ren J, Tang S, Chen T. Adaptive sliding mode control of spacecraft attitude-orbit dynamics on SE (3)[J]. Advances in Space Research, 2023, 71(1): 525-538.
[4] Ahn H, Jung D, Choi H L. Deep generative models-based anomaly detection for spacecraft control systems[J]. Sensors, 2020, 20(7): 1991.
[5] Wei C, Chen Q, Liu J, et al. An overview of prescribed performance control and its application to spacecraft attitude system[J]. Proceedings of the Institution of Mechanical Engineers, Part I: Journal of Systems and Control Engineering, 2021, 235(4): 435-447.
[6] Wu Y H, Cao X B, **ng Y J, et al. Relative motion coupled control for formation flying spacecraft via convex optimization[J]. Aerospace Science and Technology, 2010, 14(6): 415-428.
[7] Wang J, Sun Z. 6-DOF robust adaptive terminal sliding mode control for spacecraft formation flying[J]. Acta Astronautica, 2012, 73: 76-87.
[8] Zhang J, Ye D, Liu M, et al. Adaptive fuzzy finite-time control for spacecraft formation with communication delays and changing topologies[J]. Journal of the Franklin Institute, 2017, 354(11): 4377-4403.
[9] Lee K W, Singh S N. Quaternion-based adaptive attitude control of asteroid-orbiting spacecraft via immersion and invariance[J]. Acta Astronautica, 2020, 167: 164-180.
[10] Yefymenko N, Kudermetov R. Quaternion models of a rigid body rotation motion and their application for spacecraft attitude control[J]. Acta Astronautica, 2022, 194: 76-82.
[11] Tsiotras P, Valverde A. Dual quaternions as a tool for modeling, control, and estimation for spacecraft robotic servicing missions[J]. The Journal of the Astronautical Sciences, 2020, 67: 595-629.
[12] Lee D, Vukovich G. Robust adaptive terminal sliding mode control on SE (3) for autonomous spacecraft rendezvous and docking[J]. Nonlinear Dynamics, 2016, 83: 2263-2279.
[13] Gong K, Liao Y, Wang Y. Adaptive fixed-time terminal sliding mode control on SE (3) for coupled spacecraft tracking maneuver[J]. International Journal of Aerospace Engineering, 2020, 2020: 1-15.
[14] W. H. Chen, D. J. Balance, P. J. Gawthrop. "Optimal control of nonlinear systems: A predictive control approach", Automatica 39(4), 633–641 (2003)
[15] AM Shafei;H Mirzaeinejad;. (2020). A novel recursive formulation for dynamic modeling and trajectory tracking control of multi-rigid-link robotic manipulators mounted on a mobile platform . Proceedings of the Institution of Mechanical Engineers, Part I: Journal of Systems and Control Engineering, (), –. doi:10.1177/0959651820973900
[16] Iannelli P, Angeletti F, Gasbarri P. A model predictive control for attitude stabilization and spin control of a spacecraft with a flexible rotating payload[J]. Acta Astronautica, 2022, 199: 401-411.
[17] Leomanni M, Bianchini G, Garulli A, et al. Sum-of-norms MPC for linear periodic systems with application to spacecraft rendezvous[C]//2020 59th IEEE Conference on Decision and Control (CDC). IEEE, 2020: 4665-4670.
[18] Mata S, Zubizarreta A, Cabanes I, et al. Linear time varying model based model predictive control for lateral path tracking[J]. International Journal of Vehicle Design, 2017, 75(1-4): 1-22.
[19] Golzari A, Pishkenari H N, Salarieh H, et al. Quaternion based linear time-varying model predictive attitude control for satellites with two reaction wheels[J]. Aerospace Science and Technology, 2020, 98: 105677.
[20] Petersen C D, Leve F, Kolmanovsky I. Model predictive control of an underactuated spacecraft with two reaction wheels[J]. Journal of Guidance, Control, and Dynamics, 2017, 40(2): 320-332.
[21] Liu J, Li H. Artificial potential function safety and obstacle avoidance guidance for autonomous rendezvous and docking with noncooperative target[J]. Mathematical Problems in Engineering, 2019, 2019.
[22] Cao L, Qiao D, Xu J. Suboptimal artificial potential function sliding mode control for spacecraft rendezvous with obstacle avoidance[J]. Acta Astronautica, 2018, 143: 133-146.
[23] He S, Dai S L, Zhao Z, et al. UDE-Based Distributed Formation Control for MSVs With Collision Avoidance and Connectivity Preservation[J]. IEEE Transactions on Industrial Informatics, 2023.

WENBANG WANG is currently pursuing the B.E. degree with the Hubei University of Technology (HBUT), Wuhan, under the supervision of Dr. Wei Shang.He helped to complete a lot of jobs of spacecrafts, which include optimal control, attitude control, and trajectory tracking.

XIAOKANG PENG received a master's degree. He received his master's degree in Aerospace Science and Technology from Beijing Institute of Technology in 2015. Now he is an engineer of Shanghai Mechanical and Electrical Engineering Institute. His research interest covers guidance law design and optimal control theory

JIA AI is a lecturer, 33 years old, works at Wuhan Railway Vocational and Technical College. His research interests include algorithm optimization, multi-phase flow and numerical simulation of multi-field coupling mechanism.

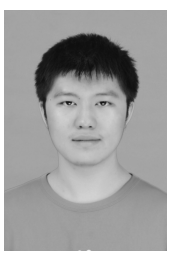

CHENG FU is currently pursuing the B.Eng. degree with the Hubei University of Technology (HBUT), Wuhan. With the help of Dr. Wei Shang, he has completed a few projects in the fields of formation control of unmanned surface vehicle, stability analysis, and visual processing. His research interests include nonlinear control systems and trajectory tracking.

CHAOBO LI is currently pursuing the B.Eng. degree with the Hubei University of Technology (HBUT), Wuhan. He is currently pursuing his research under Dr. Wei Shang, and he has completed a few projects in the fields of adaptive control and stability analysis.

ZEJIAN ZHANG is currently affiliated with the Hubei Institute of Logistics Technology as a senior engineer,Xiangyang, Hubei, China. His research interests revolve around logistics technology and computer applications.